RSC Advances

RSC Advances

PAPER

Check for updates

This article is licensed under a Creative Commons Attribution-NonCommercial 3.0 Unported Licence.

BY-NC

Synthesis of porphyrin-based 2D ytterbium metal organic frameworks for efficient photodynamic therapy†

Xiang Zheng, [ID] ‡*[abc] Jun Zhong,‡[abc] Meng-Yuan Dong,[a] Yuan Wen[abc] and Ai-Zheng Chen [ID] *[abc]

Cite this: *RSC Adv.*, 2022, **12**, 34318

Received 21st October 2022
Accepted 18th November 2022

DOI: 10.1039/d2ra06655f

rsc.li/rsc-advances

Photodynamic therapy (PDT), which relies on the photo-induced reactive oxygen species (ROS) to trigger tumor cells apoptosis, has attracted intense focus over the decades due to the minimum invasion, high-precision and controllable therapeutic processes. Tetra(4-carboxyphenyl) porphin (TCPP), as an effective PDT photosensitizer, can harness photons and generate singlet oxygen species ($^1O_2$) upon illumination; however, poor solubility and low loading rate greatly limit its further use. Although TCPP-based metal–organic-frameworks (MOFs) has been proposed to address these concerns, the relatively large size still limits their biomedical applications. Therefore, in this study, TCPP molecules are coordinated with Yb^{3+}, growing into 2D Yb-TCPP MOFs by a wet chemical method; the as-prepared Yb-TCPP MOFs are around 200 nm in size and possess high $^1O_2$ generation efficiency with low cytotoxicity. Due to TCPP is appeared as the organic frameworks of Yb-TCPP MOFs, the low loading rate problem is largely addressed; in addition, the absorbance of Yb-TCPP MOFs has been greatly expanded compared with free TCPP molecules due to the coordination with Yb^{3+}, allowing the illumination at longer wavelength range, *e.g.* 655 nm, that possesses high penetration depth and low phototoxicity. Overall, we have prepared 2D Yb-TCPP MOFs suitable for the *in vitro* anticancer effect, revealing the potential of Yb-TCPP MOFs as the future anticancer agent.

1. Introduction

The local-precision, feasibility and excellent therapeutic effect offered by photodynamic therapy (PDT) have attracted lots of research attention in the past decades.[1,2] The reactive oxygen species (ROS) produced from therapeutic agents under illumination plays the key role in realizing the PDT.[3] Therefore, in most cases, the ROS production efficiency directly determines the PDT efficacy. In other words, in order to maximize PDT efficacy, the first priority is to design a rational PDT therapeutic agent with high ROS generation efficiency.

Tetra(4-carboxyphenyl) porphin (TCPP), as an effective photosensitizer, can harness photons and generate singlet oxygen species ($^1O_2$) upon illumination, possessing great potential in PDT.[4] However, TCPP is poorly dissolved in water,

making it hard to be directly used for clinical purposes.[5] Therefore, in practice, TCPP is usually packed within drug delivery systems (DDS) to improve the solubility and bioavailability.[6] In most TCPP DDS design, the carried TCPP will be released after reaching to the lesion. Upon illumination, the released TCPP will produce $^1O_2$ to initiate PDT. For example, Kan *et al.* prepared a UiO-66-type nMOF photosensitizer (UiO-66-TPP-SH) by post-surface modification.[7] Chen *et al.* constructed a functional nanoagent (MIL-101(Fe)@TCPP) by covalently binding a porphyrin photosensitizer on MIL-101(Fe) MOF nanoparticles.[8] Many efforts have been made, nevertheless, TCPP loading rate is still far from satisfactory, restricting it from practical application.

In recent decades, metal organic frameworks (MOFs) has drawn intensive focus due to the flexible design strategies.[9,10] In MOFs, metal ions are distributed at the nodes, while organic ligands are coordinated with metal nodes and act as frameworks in 3D structure.[11] In MOFs, organic ligands and metal ions are highly replaceable, as long as the coordination and 3D periodic structure can be realized. As for TCPP, each molecule contains three carboxylic groups, which possess strong coordination ability with metal ions. Theoretically, TCPP can form MOFs with proper metal ions and synthetic strategy. Henceforth, TCPP MOFs with various metal ions as nodes have been synthesized and explored. For example, Wan *et al.* constructed

[a]College of Chemical Engineering, Huaqiao University, Xiamen 361021, P. R. China. E-mail: zhengxiang@hqu.edu.cn; azchen@hqu.edu.cn; Tel: +86-592-616-2326

[b]Institute of Biomaterials and Tissue Engineering, Huaqiao University, Xiamen 361021, P. R. China

[c]Fujian Provincial Key Laboratory of Biochemical Technology (Huaqiao University), Xiamen 361021, P. R. China

† Electronic supplementary information (ESI) available. See DOI: https://doi.org/10.1039/d2ra06655f

‡ These authors contribute equally.

34318 | *RSC Adv.*, 2022, **12**, 34318–34324

© 2022 The Author(s). Published by the Royal Society of Chemistry

a metal–organic framework (MOF) nanosystem based on the coordination of Mn(III) and porphyrin (TCPP), with controllable ROS generation and GSH depletion, which can significantly improve the efficacy of photodynamic therapy.[12] Wang *et al.* synthesized 2D Cu-TCPP nanosheets by reacting with H_2O_2 to generate $^1O_2$ and cyclically consume GSH.[13] TCPP MOFs largely addressed the low loading rate of TCPP in DDS, as TCPP is now no longer a cargo but the framework of the nanostructure, therefore the low loading rate problem is largely alleviated. In addition, since TCPP is fitted within MOFs 3D structures, the molecular movement freedom (vibration, rotation, stretching *etc.*) is largely restricted, it is also reported that the formation of TCPP MOFs can significantly reduce the self-quenching problem of free TCPP molecules, thus improving the overall PDT efficiency.[14–16] Although many efforts have been made in the development of TCPP MOFs, some TCPP-based MOFs still lack systematic study. For example, ytterbium (Yb), which is an important lanthanide element with highly simplified isolated energy levels and high biocompatibility.[17] However, the application of lanthanide-TCPP MOFs, especially Yb-TCPP MOFs, has mostly been limited in the field of catalysis, sensing and energy, while the biomedical application has been missing, with one of the major reasons being the relatively large size.[18,19]

Therefore, in this study, we prepared nanosized Yb-TCPP MOFs and perform related characterization to evaluate the $^1O_2$ production ability and PDT efficacy *in vitro*. To begin with, nanoscale Yb-TCPP MOFs are prepared by a relatively simple wet chemical methods with uniformly distributed size and 2D morphology, the as-prepared Yb-TCPP MOFs are around 200 nm in size, which are much smaller than previously reported ones. The small size is highly beneficial to the following *in vitro* test of $^1O_2$ production ability and PDT efficacy. To guide the following $^1O_2$ generation test, the maximum absorbance of free TCPP and Yb-TCPP is obtained by using a UV-Vis spectrometer. Then, Yb-TCPP $^1O_2$ production is characterized by using 1,3-diphenylisobenzofuran (DPBF). Under 655 nm illumination, the quick degradation of DPBF indicate the excellent $^1O_2$ production ability of Yb-TCPP. Finally, Yb-TCPP MOFs are sent for *in vitro* test to examine the cell toxicity and PDT efficacy. With low cytotoxicity and high efficacy, this study highlights the superiority of Yb-TCPP MOFs in cancer treatment and provide a feasible Yb-TCPP MOFs preparation strategy. In addition, the Yb^{3+} ions incorporated in the MOFs could be further developed to possess other biomedical features which could be coupled with TCPP to achieve combined therapy.

2. Experimental

Materials

1,3-Diphenylisobenzofuran (DPBF), fluorescein isothiocyanate isomer (FITC) were obtained from Admas-beta Reagents Company (Shanghai, China). Dulbecco's modified Eagle's medium (DMEM) was purchased from Solarbio Life Science (Beijing, China). Calcein AM/PI Double Stain Kit, 2,7-dichlorodihydrofluorescein diacetate (DCFH-DA), and Cell Counting Kit-8 (CCK-8) were obtained from Beyotime Biotechnology Co. Ltd. (Shanghai, China).

Measurements and characterizations

The size and morphology of the samples were characterized by TEM (JEM-2010, 200 kV), HAADF-STEM (JEM-2100F), field-emission scanning electron microscopy (FESEM; Hitachi, SU5000). Confocal laser scanning microscopy (CLSM) images were obtained with confocal microscopy (Leica TCS SP8). The crystal information of the samples is established using XRD (Bruker-D8 Advance) with Cu-Kα radiation. The-apoptosis rate of 4T1 cells was analyzed with AnnexinV-FITC/PI-double-staining.

Detection of $^1O_2$ generation in solution with DPBF probe

First, 10 mg of DPBF was dissolved in 10 mL of ethanol, and then 50 μL of this solution was added to an aqueous Yb-TCPP dispersion (100 μg mL^{-1}, 5 ml). Then, the solution was irradiated with 655 nm laser for 10 min, and the absorbance at 410 nm was measured with a UV-Vis absorption spectrophotometer every 2 min.

In vitro cytotoxicity assay using the CCK-8 protocol

Cell viability was determined using the CCK-8 method. 4T1 cells were seeded into 96-well plates, the number of cells in each well was kept at 1×10^3, and cultured in an incubator for 12 h. After the medium in the well plate was aspirated, DMEM containing PBS and Yb-TCPP were then added to each well, and incubated for another 8 h. Subsequently, the Yb-TCPP-containing medium was irradiated with a 655 nm laser for 10 min. The cells were further cultured for 16 h. Finally, the medium solution containing the nanomaterials was aspirated and washed three times with PBS. Then, each well was replaced with DMEM containing CCK-8 solution (100 μL, 10% CCK-8), and the cells were incubated for another 1 h, and measured its absorbance at 450 nm with a microplate reader.

Detection of intracellular $^1O_2$ production

Intracellular $^1O_2$ generation was measured with CLSM. 4T1 cells were seeded into 6-well plates, the number of cells in each well was kept at 1×10^4, and cultured in an incubator for 12 h. After the medium in the well plate was aspirated, DMEM containing PBS and Yb-TCPP were then added to each well, and incubated for another 8 h. Subsequently, the Yb-TCPP-containing medium was irradiated with a 655 nm laser for 10 min. The medium was aspirated, 0.2 μM DCFH-DA solution was added as a ROS detection probe and added to the culture dish, and incubated for another 20 min. Finally, the 4T1 cells were gently washed 3 times with PBS, and the intracellular $^1O_2$ was detected with CLSM.

Observation of live and dead cell fluorescence by CLSM

Live and dead cells were observed with CLSM, and 4T1 cells were seeded into 6-well plates, the cells in each well plate were maintained at 1×10^5. The next procedure is roughly the same as that for measuring cytotoxicity. After addition of nanomaterials and illumination, 4T1 cells were further incubated for 16 h. After removing the medium and rinsing the dishes, 4T1

cells were stained with calcein and PI, live cells were stained green and dead cells were stained red. After 15 minutes of staining, the staining solution was aspirated, and the cells were rinsed twice with PBS, and then visualized with CLSM.

3. Results and discussion

Synthesis and characterization of Yb-TCPP MOFs

The Yb-TCPP MOFs are synthesized by mixing and stirring ytterbium chloride hexahydrate (YbCl$_3$·6H$_2$O) and TCPP in *N,N*-dimethylformamide (DMF) and *n*-hexane solution containing trifluoroacetic acid, polyvinyl pyrrolidone (PVP) and triethylamine (TEA) at elevated temperature. Under SEM and TEM images, the as-prepared Yb-TCPP MOFs exhibit a 2D morphology due the binding effect of PVP during the crystal growth, where the planar growth of MOFs crystal becomes dominated (Fig. 1A and B). From XRD data and elemental mapping results, the as-prepared Yb-TCPP MOFs are well crystalized with Yb^{3+} ions evenly distributed within Yb-TCPP MOFs, indicating the successful synthesis of Yb-TCPP MOFs (Fig. 1C–H). To study the absorbance profiles and the correlation between free TCPP molecules and Yb-TCPP MOFs, UV-Vis spectrum is obtained for both. From the spectra, free TCPP molecules have sharp absorbance peaks located at 410 nm while Yb-TCPP MOFs have a much wider absorbance band, with good absorbance ability up to near-infrared region (Fig. 1I). This indicate that porphin centers of Yb-TCPP MOFs have been coordinated with Yb^{3+} ions as a result of formation of MOFs. Due to the wide absorbance band of Yb-TCPP MOFs, longer wavelength illumination can be applied in practice, which is highly favorable in therapeutics as the phototoxicity could be greatly reduced and the penetration depth could be largely improved, thus, 655 nm illumination are used to study the $^1O_2$ generation ability and PDT efficacy. Overall, materials characterization results demonstrate that the synthesis is successful, the as-prepared Yb-TCPP MOFs is thus used for the following experiments.

$^1O_2$ production test

After the successful synthesis of Yb-TCPP MOFs, the $^1O_2$ generation ability is evaluated by using $^1O_2$ detection probe (1,3-diphenylisobenzofuran, DPBF). Briefly, the presence of $^1O_2$ in
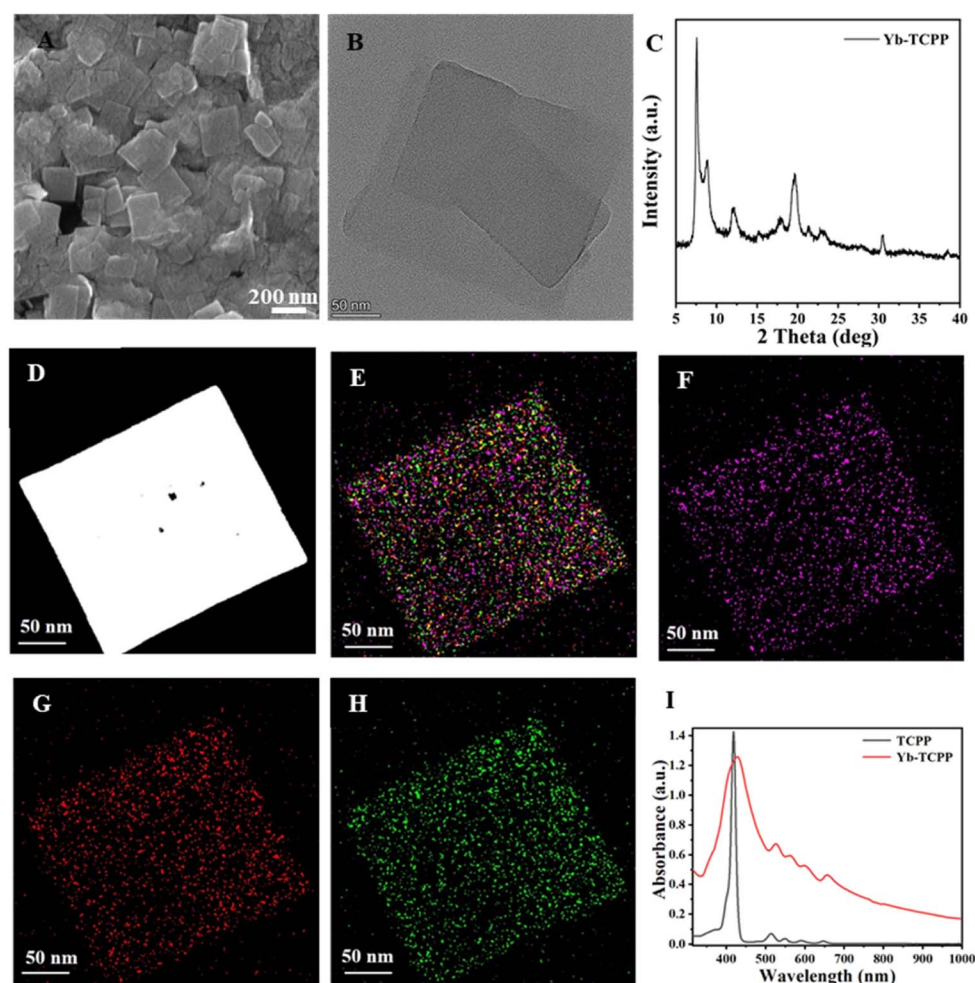

Fig. 1 Physical characterization of Yb-TCPP MOFs. (A) SEM image, (B) TEM image and (C) XRD of Yb-TCPP MOFs. (D) HAADF-STEM image of Yb-TCPP MOFs. (E) Collated elemental mapping results of (F) Yb, (G) O and (H) C of the same sample in figure (D). (I) UV-Vis absorbance curve of free TCPP molecules (black) and Yb-TCPP MOFs (red).
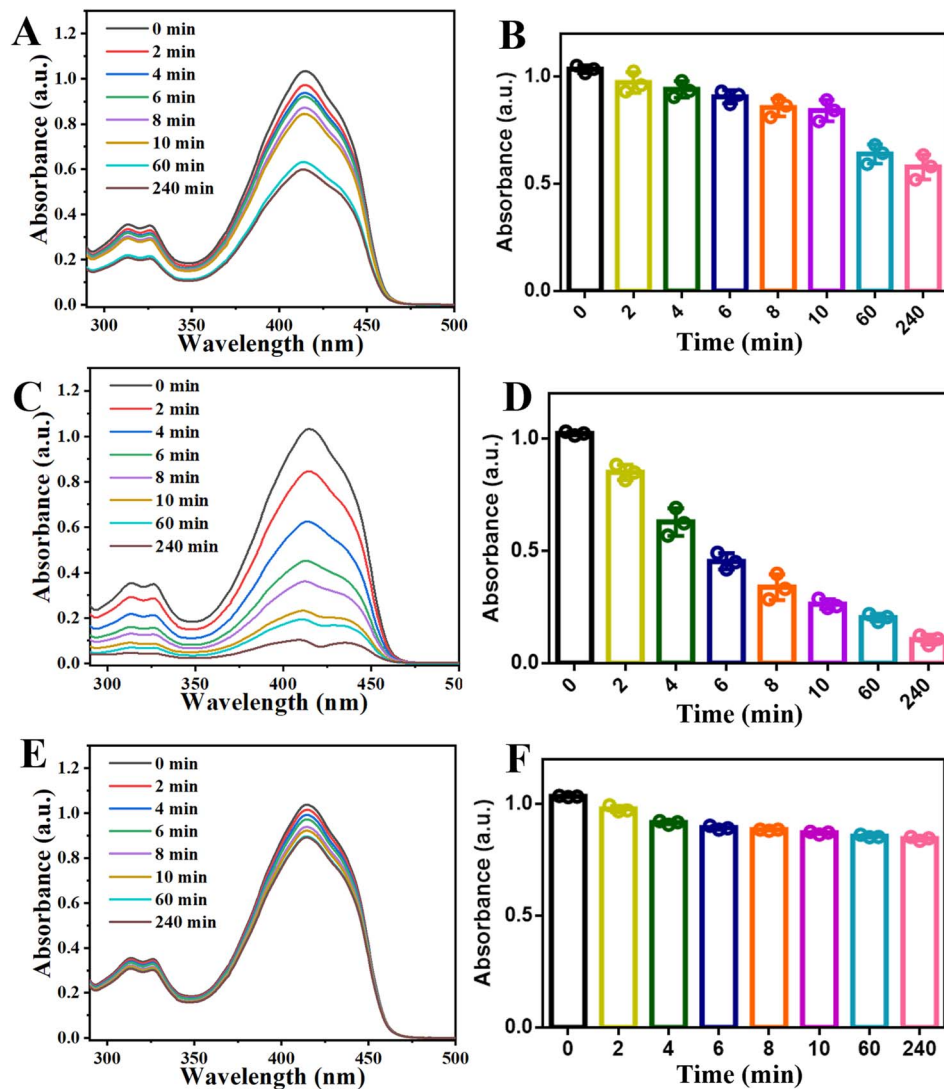
Fig. 2 UV-Vis absorbance curve of DPBF mixture under different condition. (A) UV-Vis absorbance curve of DPBF incubated with Yb–TCPP MOFs without 655 nm illumination and (B) the corresponding area integration, normalized at 0 min. (C) UV-Vis absorbance curve of DPBF incubated with Yb–TCPP MOFs under 655 nm illumination and (D) the corresponding area integration, normalized at 0 min. (E) UV-Vis absorbance curve of DPBF incubated with TCPP molecules under 655 nm illumination and (F) the corresponding area integration, normalized at 0 min.

the environment will quickly degrade the DPBF, which can be reflected on the decrement of UV-Vis absorbance spectra. Thus, the $^1O_2$ generation can be deduced by comparing the UV-Vis spectra of the mixture. Therefore, DPBF is introduced into Yb–TCPP MOFs suspension. Without 655 nm illumination, from UV-Vis spectra, slight reduction of absorbance curve is observed for Yb–TCPP MOFs, due to the $^1O_2$ produced under Russsel mechanism (Fig. 2A and B). When Yb–TCPP MOFs are illuminated with 655 nm light, UV-Vis absorbance curves are reduced at a much faster speed, indicating the quick and efficient generation of $^1O_2$ (Fig. 2C and D). As the illumination continuous, the UV-Vis absorbance keeps decreasing, showing the stable $^1O_2$ generation ability of Yb–TCPP MOFs which will not be bleached with up to 4 hours illumination (Fig. 2D). The stable $^1O_2$ production behaviour also indicate the high photostability during the whole illumination period up to 4 h. On the contrary, due to the poor absorbing ability at longer wavelength region

and self-quenching problem of free TCPP molecules, under 655 nm illumination, the decay absorbance curve is negligible in the 4 hour timescale (Fig. 2E and F), which further supports the superiority of Yb–TCPP MOFs as the PDT agent. The excellent $^1O_2$ production of Yb–TCPP MOFs lays the foundation for following *in vitro* PDT experiments.

In addition, to guarantee the breakdown of Yb–TCPP MOFs will not happen upon illumination, Yb–TCPP MOFs are placed under 655 nm illumination with maximum power density for 1 h to evaluate the photostability under extreme condition. Results show that, Yb–TCPP MOFs still possess good $^1O_2$ production ability as the absorbance of DPBF suspension quickly dropped once introduced to the Yb–TCPP MOFs suspension and illuminated with 655 nm light (Fig. S1†); in addition, no observable degradation or damage of structure is captured on TEM image (Fig. S2†).
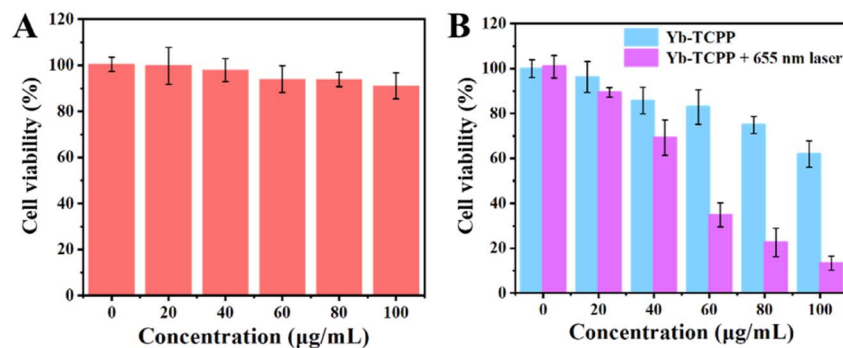
Fig. 3 Biocompatibility and PDT experiments. (A) Cell viability of 3T3 cell incubated with different concentration of Yb-TCPP MOFs. (B) 4T1 tumor cell death rate incubated with different concentration of Yb-TCPP MOFs under 655 nm illumination for 10 min.
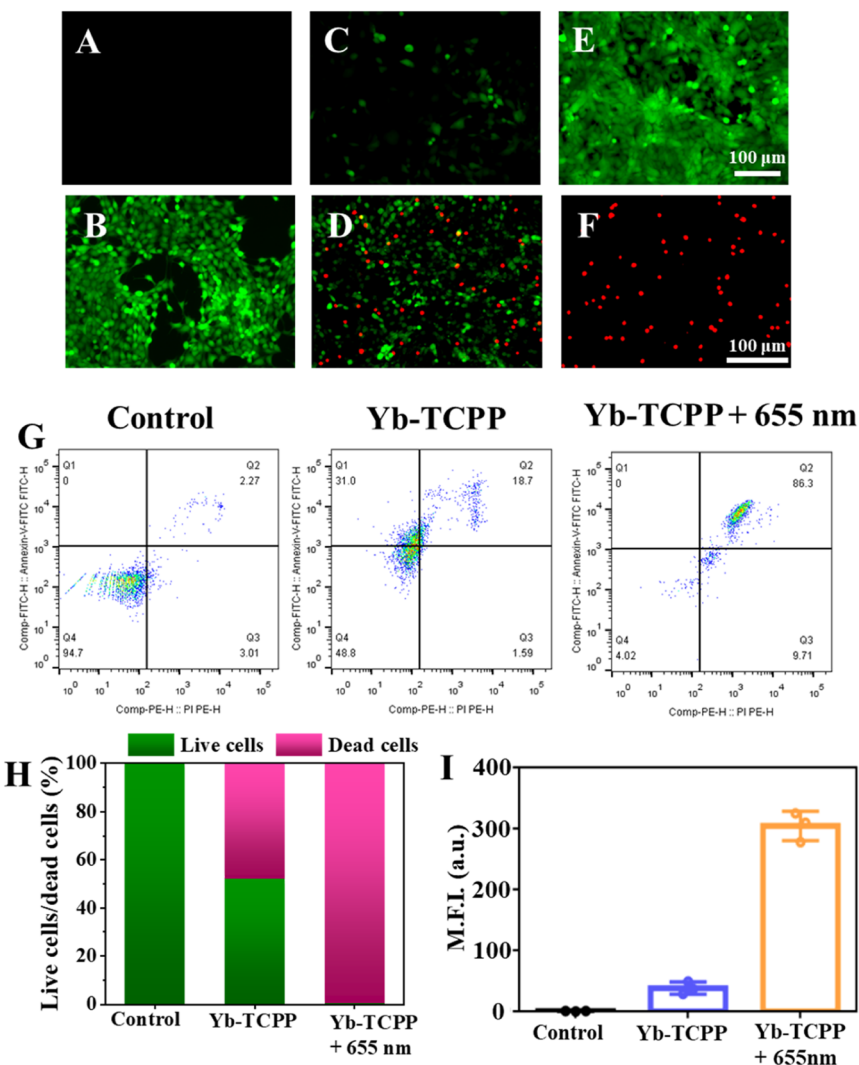

Fig. 4 *In vitro* CLSM image of calcein AM/PI Double Stain Kit and DCFH-DA treated 4T1 tumor cells revealing the $^1O_2$ generation and 4T1 tumor cells survival condition. (A) DCFH-DA and (B) calcein AM/PI treated 4T1 tumor cells without Yb-TCPP MOFs as control group. (C) DCFH-DA and (B) calcein AM/PI treated 4T1 tumor cells incubated with Yb-TCPP MOFs without illumination. (E) DCFH-DA and (F) calcein AM/PI treated 4T1 tumor cells incubated with Yb-TCPP MOFs under 655 nm illumination for 10 min. (G) Apoptotic analysis of 4T1 cells from above three groups by flow cytometry. (H) Overall fluorescence intensity of live/death staining. (I) Overall intensity of fluorescence from DCFH-DA induced by environmental $^1O_2$.

In vitro PDT assessment

After establishing and confirming the excellent $^1O_2$ generation ability of Yb-TCPP MOFs, we move on to explore the *in vitro* anti-cancer effects of Yb-TCPP MOFs. The experiments begin with the biocompatibility and cytotoxicity test of Yb-TCPP MOFs by using 3T3 cells as the indicators. 3T3 cells are incubated with different amount of Yb-TCPP MOFs. In the 24 h-incubation period, 3T3 cells can still maintain a high survival rate (Fig. 3A). Even with 100 μg per mL Yb-TCPP MOFs addition amount, more than 90% 3T3 cells are still alive, indicating that Yb-TCPP MOFs exhibit low cytotoxicity and high biocompatibility, suitable for the further therapeutic applications. Subsequently, 4T1 cancer cells are used to evaluate the anti-cancer effect of Yb-TCPP MOFs. 4T1 cells are cocultured with different amounts of Yb-TCPP MOFs. Without 655 nm illumination, Yb-TCPP MOFs do not exhibit noticeable kill effect on 4T1 cancer cells (Fig. 3B); however, due to the relatively high level of H_2O_2 in cancel cells, Yb-TCPP MOFs can still present anti-cancer effect due to the Russell mechanism, still, only 30% 4T1 cells are dead at a concentration as high as 100 μg mL^{-1} (Fig. 3B). On the contrary, with 10 min 655 nm illumination, more than 80% 4T1 cells are quickly killed, due to the large amount of $^1O_2$ produced by during PDT, inducing significant oxidative damage to cells, causing 4T1 tumor cells apoptosis.

To further verify the anti-cancer effect of Yb-TCPP MOFs is due to the $^1O_2$ produced under illumination, calcein AM/PI double stain kit is applied to reveal the live/death status of cells, simultaneously, 2,7-dichlorodihydrofluorescein diacetate (DCFH-DA) is applied to evaluate the $^1O_2$ within cells in a more intuitive way. From confocal laser scanning microscope (CLSM) image, in the control group, where the Yb-TCPP MOFs is missed, no green fluorescence is received, indicating no $^1O_2$ is generated (Fig. 4A). Correspondingly, in the live/dead staining test, 4T1 tumor cells are mostly alive (Fig. 4B). When Yb-TCPP MOFs are added to the system, without illumination, only traceable green fluorescence is captured, indicating small amount of $^1O_2$ is generated *via* the Fenton-like mechanism in the H_2O_2-rich environment within tumor cells (Fig. 4C). However, as the $^1O_2$ level is low, only a few 4T1 cells lose the vitality, with traceable red fluorescence appeared (Fig. 4D). Finally, when 655 nm illumination is applied to activate PDT, strong green fluorescence can be detected under CLSM, indicating the high $^1O_2$ production efficiency (Fig. 4E). Correspondingly, under live/death staining experiment, 4T1 cells are mostly killed in $^1O_2$ rich environment, indicating the PDT is highly effective (Fig. 4F).

The apoptotic cells of the three groups are further measured by flow-cytometry using AnnexinV-FITC/PI-double-staining tool kit to statistically analyse the cells status in a more quantifiable manner. It is obvious that 655 nm +Yb-TCPP MOFs treatment group has the highest ratio of apoptotic cells, much higher than Yb-TCPP group with 655 nm illumination, while the control group has no observable anticancer effect (Fig. 4g). Live/death staining also reveals the similar tread, with 655 nm +Yb-TCPP MOFs treatment group has the highest death rate (Fig. 4H), in addition, the highly correlated $^1O_2$ production efficiency and anti-cancer effect indicate that the major anticancer mechanism is $^1O_2$-induced apoptosis (Fig. 4I).

4.   Conclusions

In this study, Yb-TCPP MOFs are prepared with a relatively simple wet chemical method. The as-prepared Yb-TCPP MOFs exhibit a 2D morphology, with relatively small size at around 200 nm. XRD and elemental analysis reveals the well-crystalized structures with Yb^{3+} ions evenly distributed within, indicating the successful synthesis of Yb-TCPP MOFs. UV-Vis absorbance of Yb-TCPP MOFs shows a wide absorbance band in visible range compared with free TCPP molecules, which only have a narrow absorption peak located at short wavelength range. The broadening of absorbance peak is largely due to the coordination between TCPP and Yb^{3+}. Compared with free TCPP molecules, Yb-TCPP MOFs exhibit good absorbance ability in long wavelength range, *e.g.* 655 nm, which is highly favorable in therapeutic applications due to the deep penetration ability and low phototoxicity. Subsequently, the $^1O_2$ production of TCPP and Yb-TCPP MOFs under 655 nm illumination is studied by using DPBF. The excellent $^1O_2$ production efficiency of Yb-TCPP MOFs lays the foundation for the further *in vitro* PDT test; meanwhile, it also supports the superiority of Yb-TCPP MOFs in enhancing $^1O_2$ production efficiency. Finally, *in vitro* biocompatibility and PDT efficacy studies are performed. Cytotoxicity experiments show the high biocompatibility of Yb-TCPP MOFs, with more than 90% 3T3 cells remain alive under 100 μg per mL Yb-TCPP MOFs concentration. When co-cultured with 4T1 tumor cells, with only 10 min 655 nm illumination, more than 80% of cancer cells are quickly killed. The highly correlated tumor cell death rate and $^1O_2$ level directly supports the Yb-TCPP MOFs induced PDT is the primary anti-cancer mechanism. The successful synthesis of nanoscale 2D Yb-TCPP MOFs, high $^1O_2$ production efficiency, low cytotoxicity and excellent PDT efficacy highlights the superiority of Yb-TCPP MOFs in biomedical, serving as a new powerful weapon in the fight against cancer and other disease.

Author contributions

Conceptualization, Xiang Zheng; Data curation, Jun Zhong and Meng-Yuan Dong; Formal analysis, Jun Zhong; Funding acquisition, Ai-Zheng Chen; Investigation, Jun Zhong, Meng-Yuan Dong and Yuan Wen; Project administration, Xiang Zheng and Ai-Zheng Chen; Supervision, Xiang Zheng; Visualization, Yuan Wen; Writing – original draft, Xiang Zheng; Writing – review & editing, Xiang Zheng.

Conflicts of interest

The authors declare no competing financial interest.

Acknowledgements

References

1 S.-S. Wan, J.-Y. Zeng, H. Cheng and X.-Z. Zhang, ROS-induced NO generation for gas therapy and sensitizing photodynamic therapy of tumor, *Biomaterials*, 2018, **185**, 51–62.

2 D. E. J. G. J. Dolmans, D. Fukumura and R. K. Jain, Photodynamic therapy for cancer, *Nat. Rev. Cancer*, 2003, **3**(5), 380–387.

3 D. Chen, Q. Xu, W. Wang, J. Shao, W. Huang and X. Dong, Type I Photosensitizers Revitalizing Photodynamic Oncotherapy, *Small*, 2021, **17**(31), 2006742.

4 J. Park, Q. Jiang, D. Feng, L. Mao and H.-C. Zhou, Size-Controlled Synthesis of Porphyrinic Metal–Organic Framework and Functionalization for Targeted Photodynamic Therapy, *J. Am. Chem. Soc.*, 2016, **138**(10), 3518–3525.

5 C. Liang, L. Xu, G. Song and Z. Liu, Emerging nanomedicine approaches fighting tumor metastasis: animal models, metastasis-targeted drug delivery, phototherapy, and immunotherapy, *Chem. Soc. Rev.*, 2016, **45**(22), 6250–6269.

6 D. Bechet, P. Couleaud, C. Frochot, M.-L. Viriot, F. Guillemin and M. Barberi-Heyob, Nanoparticles as vehicles for delivery of photodynamic therapy agents, *Trends Biotechnol.*, 2008, **26**(11), 612–621.

7 J.-L. Kan, Y. Jiang, A. Xue, Y.-H. Yu, Q. Wang, Y. Zhou and Y.-B. Dong, Surface Decorated Porphyrinic Nanoscale Metal–Organic Framework for Photodynamic Therapy, *Inorg. Chem.*, 2018, **57**(9), 5420–5428.

8 X. B. Wang, C. Y. Li, Z. Y. Li, X. Ma, D. K. Chen, X. Y. Wan, Z. Deng, R. R. Deng and X. S. Peng, Near-Infrared-Light emitting diode driven white light emission: upconversion nanoparticles decorated Metal-Organic Frame-works thin film, *Chem. Eng. J.*, 2021, 409.

9 H. Furukawa, K. E. Cordova, M. O'Keeffe and O. M. Yaghi, The Chemistry and Applications of Metal-Organic Frameworks, *Science*, 2013, **341**(6149), 1230444.

10 H.-C. Zhou, J. R. Long and O. M. Yaghi, Introduction to Metal–Organic Frameworks, *Chem. Rev.*, 2012, **112**(2), 673–674.

11 J. Zhou, T. Ke, F. Steinke, N. Stock, Z. Zhang, Z. Bao, X. He, Q. Ren and Q. Yang, Tunable Confined Aliphatic Pore Environment in Robust Metal–Organic Frameworks for Efficient Separation of Gases with a Similar Structure, *J. Am. Chem. Soc.*, 2022, **144**(31), 14322–14329.

12 S.-S. Wan, Q. Cheng, X. Zeng and X.-Z. Zhang, A Mn(III)-Sealed Metal–Organic Framework Nanosystem for Redox-Unlocked Tumor Theranostics, *ACS Nano*, 2019, **13**(6), 6561–6571.

13 C. Wang, F. Cao, Y. Ruan, X. Jia, W. Zhen and X. Jiang, Specific Generation of Singlet Oxygen through the Russell Mechanism in Hypoxic Tumors and GSH Depletion by Cu-TCPP Nanosheets for Cancer Therapy, *Angew. Chem., Int. Ed.*, 2019, **58**(29), 9846–9850.

14 C. Y. Lee, O. K. Farha, B. J. Hong, A. A. Sarjeant, S. T. Nguyen and J. T. Hupp, Light-Harvesting Metal–Organic Frameworks (MOFs): Efficient Strut-to-Strut Energy Transfer in Bodipy and Porphyrin-Based MOFs, *J. Am. Chem. Soc.*, 2011, **133**(40), 15858–15861.

15 T. Zhang and W. Lin, Metal–organic frameworks for artificial photosynthesis and photocatalysis, *Chem. Soc. Rev.*, 2014, **43**(16), 5982–5993.

16 K. Lu, C. He and W. Lin, Nanoscale Metal–Organic Framework for Highly Effective Photodynamic Therapy of Resistant Head and Neck Cancer, *J. Am. Chem. Soc.*, 2014, **136**(48), 16712–16715.

17 J. Ren, Z. Niu, Y. Ye, C.-Y. Tsai, S. Liu, Q. Liu, X. Huang, A. Nafady and S. Ma, Second-Sphere Interaction Promoted Turn-On Fluorescence for Selective Sensing of Organic Amines in a TbIII-based Macrocyclic Framework, *Angew. Chem., Int. Ed.*, 2021, **60**(44), 23705–23712.

18 Z. W. Jiang, Y. C. Zou, T. T. Zhao, S. J. Zhen, Y. F. Li and C. Z. Huang, Controllable Synthesis of Porphyrin-Based 2D Lanthanide Metal–Organic Frameworks with Thickness- and Metal-Node-Dependent Photocatalytic Performance, *Angew. Chem., Int. Ed.*, 2020, **59**(8), 3300–3306.

19 Z. W. Jiang, T. T. Zhao, S. J. Zhen, C. M. Li, Y. F. Li and C. Z. Huang, A 2D MOF-based artificial light-harvesting system with chloroplast bionic structure for photochemical catalysis, *J. Mater. Chem. A*, 2021, **9**(14), 9301–9306.